ELSEVIER

Journal of Structural Geology 28 (2006) 549–560

JOURNAL OF STRUCTURAL GEOLOGY

www.elsevier.com/locate/jsg

Multiscale anisotropy controlled by folding: the example of the Chaudrons fold (Corbières, France)

Laurent Louis [a,b,*], Philippe Robion [a], Christian David [a], Dominique Frizon de Lamotte [a]

[a] *Université de Cergy-Pontoise, Département des Sciences de la Terre et de l'Environnement, UMR CNRS 7072, Bâtiment Neuville 3.1, 5 mail Gay Lussac, F-95031 Cergy-Pontoise, France*

[b] *Stony Brook University, Department of Geosciences, Stony Brook, NY 11794-2100, USA*

Received 21 August 2005; received in revised form 16 January 2006; accepted 20 January 2006
Available online 10 March 2006

Abstract

In this paper, anisotropies developed in silicoclastic continental deposits during the building of the Chaudrons anticline (Corbières, France) are studied. A microstructural analysis of the deformational features in three different panels within the fold (crest, hinge, and forelimb, respectively) is reported and compared with early field observations (distribution and orientation of cleavage) and laboratory measurements (estimation of magnetic and acoustic anisotropies). The main finding of this investigation is the preservation of unwelded joints between grains of calcite promoted by the presence of quartz grains. These joints, which appear as discontinuities in a matrix of calcite, are analyzed in orientation and composition. In the three panels of the fold that are investigated, a range of dip angles is observed with at least two major generations of joints, the average orientation of which is found to be consistent with both macroscopic cleavage and magnetic and acoustic fabrics. To account for the multimodal distribution of the joints orientation, we suggest an original scenario in which they are successively generated by sets. Two processes have operated simultaneously during the development of the fold: (1) horizontal rock mass compaction inducing pressure solution and twinning in calcite; (2) preservation of unwelded calcite/calcite grain joints due to stress heterogeneities associated with quartz inclusions. From these results, we suggest that microstructural processes are the same before and during folding, ruling out a passive shearing of cleavage plane formed during a first step of layer parallel shortening.

Keywords: Anisotropy; Magnetic susceptibility; P-wave velocity; Pressure solution; Cleavage

1. Introduction

Studies of regional structures have often considered that microstructures were not taking on a significant part of plastic strain during folding, arguing that if affected they would be so mostly during early pre-folding stages like burial related compaction or layer parallel shortening (LPS). In the Barclay fold, Thorbjornsen and Dunne (1997) observed that original microstructures had not been significantly disturbed during folding, while other studies revealed some strain-related textures that were attributed to LPS only: see the example of the Lagrasse fold (Corbières, France) (Averbuch et al., 1992; Frizon de Lamotte et al., 1997), or the work of Tavarnelli (1997) in the Apennines (Italy). Still, it was shown in a few examples that microstructures were at least partly sin-folding: in the Tadighoust anticline (High Atlas, Morocco) (Saint-Bézar et al., 2002), in the Oupia anticline (Corbières, France) (Grelaud et al., 2000), or in the Lost River Range (Idaho, USA) (Anastasio et al., 1997). In order to understand better the relationships between micro-/mesoscopic deformation patterns and the kinematic or mechanical evolution of a fold, more case studies are required.

The Chaudrons anticline (Corbières, France) provides a good opportunity for such a work mainly for two reasons: first, due to a weak (even naught) compaction, meso-scale tectonic features (fractures, cleavage) are particularly well expressed (Ellenberger, 1967; Cluzel, 1977; Averbuch et al., 1992; Frizon de Lamotte et al., 2002; Tavani et al., 2004); second, the orientation of these features with respect to the bedding depend on their location in the fold and are consequently folding-related (Tavani et al., 2004).

The purpose of this study is to understand how and at which scale strain was accommodated during the construction of the Chaudrons fold, with a particular emphasis on the role of microstructures. This work was largely motivated by

* Corresponding author. Tel.: +1 631 632 8302; fax: +1 631 632 8240.
E-mail address: llouis@notes.cc.sunysb.edu (L. Louis).

0191-8141/$ - see front matter © 2006 Elsevier Ltd. All rights reserved.
doi:10.1016/j.jsg.2006.01.002

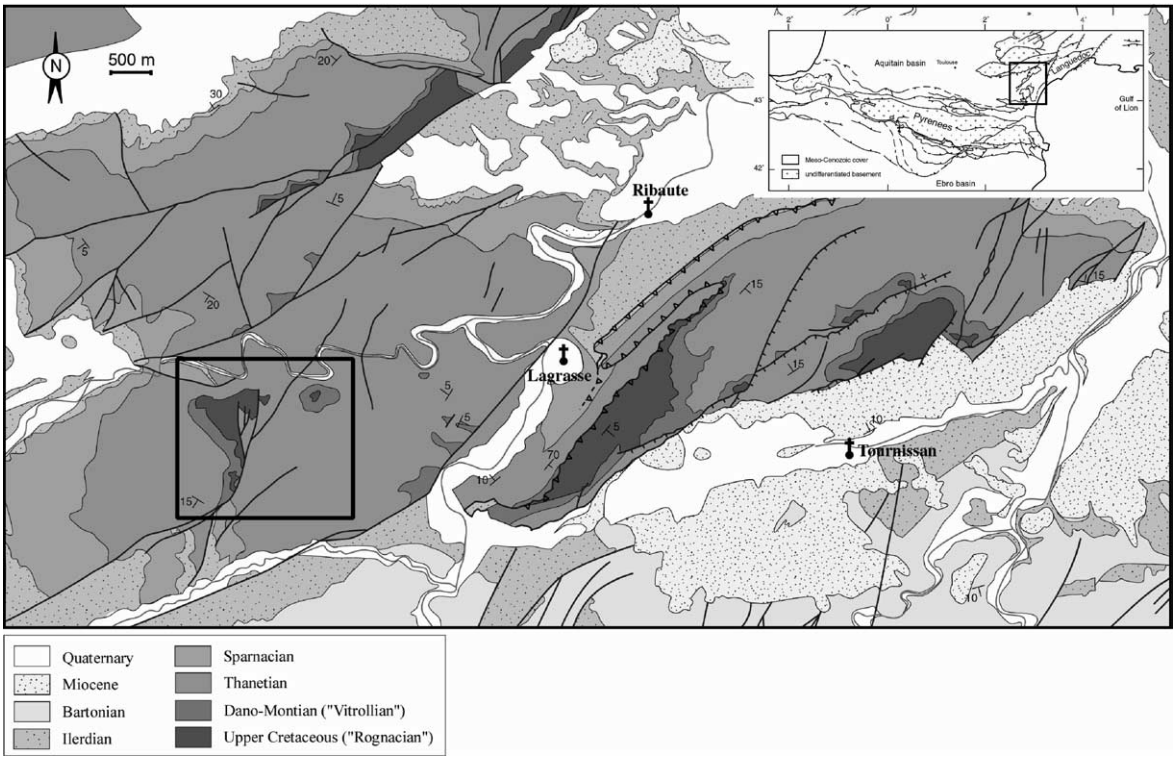

Fig. 1. Location of the area studied (after Souque et al., 2002). The Chaudrons fold belongs to the Corbières transfer zone, which binds the North Pyrenean zone to the Languedoc–Provence thrust belt.

the observations and measurements reported in Tavani et al. (2004). In this respect, it seeks to complete the description of the fold with a section on microstructures. We propose in the following to compare the deformational features displayed by the fold at three different scales (outcrop, laboratory sample, and microscale) and in three different parts of the Chaudrons fold (crest, hinge, and forelimb). While outcrop- and micro-scale results arise from direct observation, the

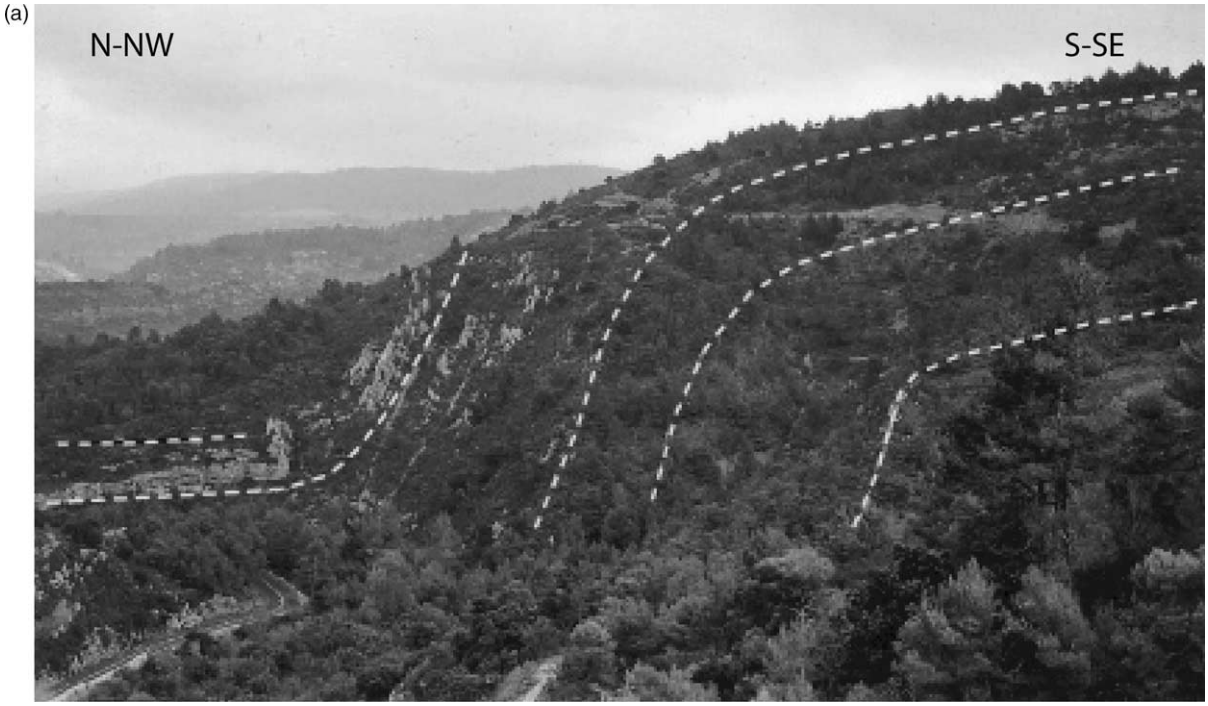

Fig. 2. Outcrop photographs within the Chaudrons fold. (a) Whole section showing from the left the forelimb, the hinge and part of the crestal zones (photograph looking eastward). In the lower left side, the road indicates scale. (b) Into the crest, the bedding (S0) is nearly normal to the cleavage (S1). (c) Into the hinge, the cleavage rotates less than the bedding.

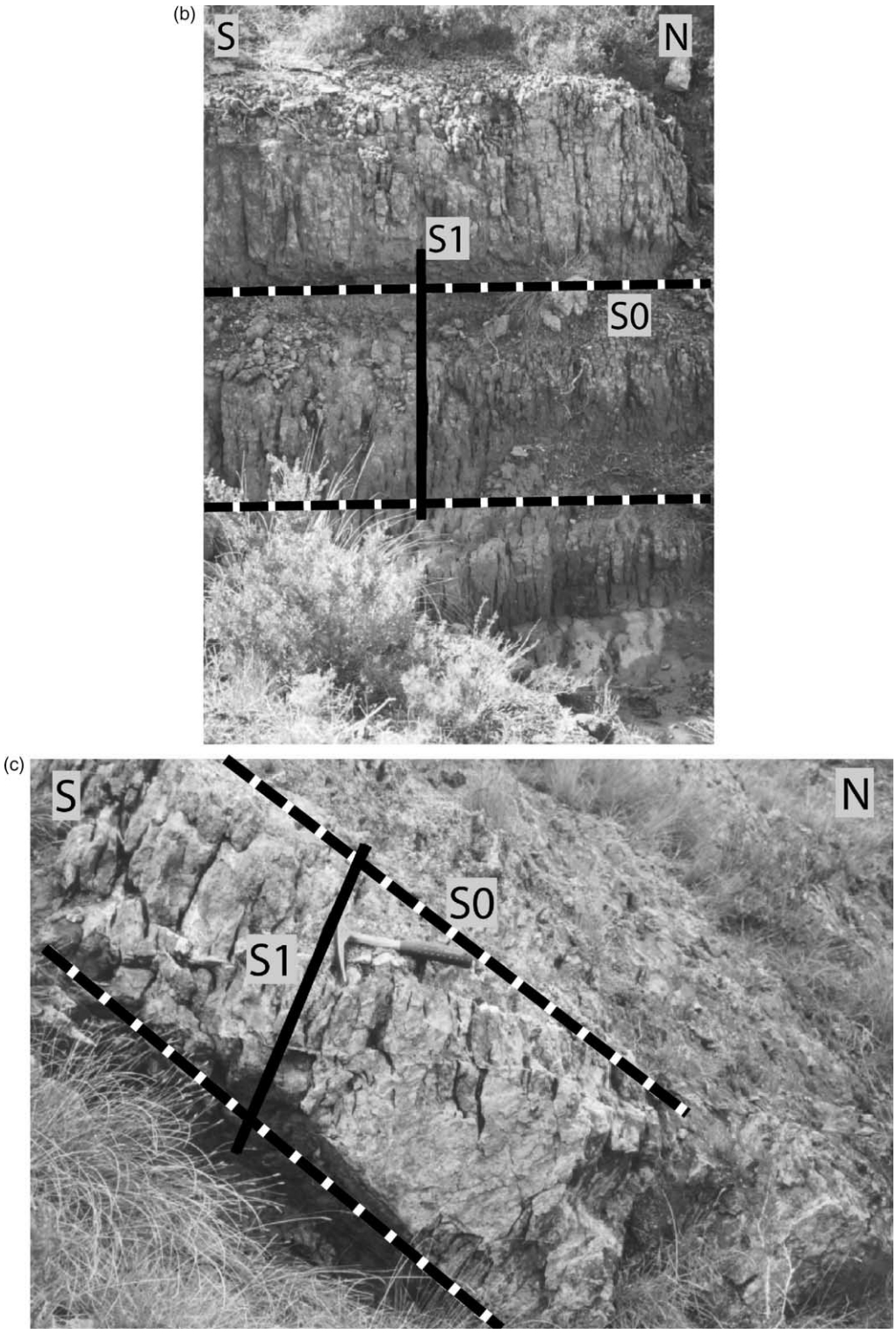

Fig. 2 (*continued*)

sample-scale analysis is achieved through the estimation of the anisotropy of magnetic susceptibility and P-wave velocity (referred to hereafter as AMS and APV, respectively), following the method introduced in Louis et al. (2004). Eventually, a sketch describing the sequential development of the cleavage along with the building of the Chaudrons fold is proposed.

2. Geological setting

The 'Chaudrons' fold belongs to the French Corbières fold–thrust belt, which forms an arc joining the North Pyrenean zone and the Languedoc–Provence thrust belt (Ellenberger, 1967) (Fig. 1). This domain is characterized by a relatively thin sedimentary cover about 1000 m of lacustrine limestone,

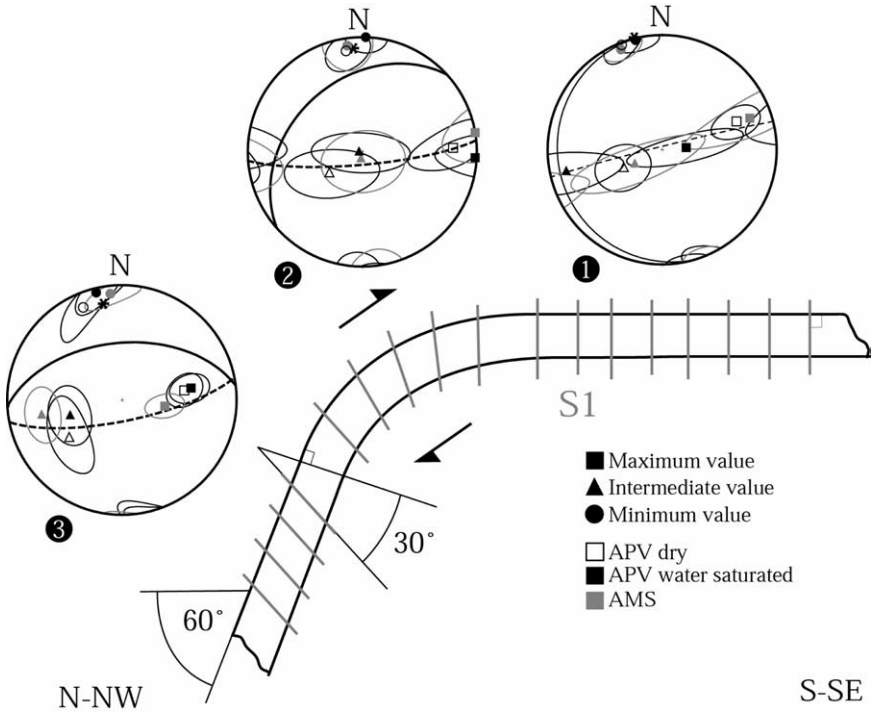

Fig. 3. Synthetic transect of the fold showing the three deformation panels isolated by Tavani et al. (2004): (1) crest of the fold; (2) transition from crest to forelimb; (3) forelimb. The figure displays both bedding (S0) and cleavage (S1) orientations along the fold and stereoplots resulting from AMS (gray symbols) and APV (black symbols) measurements. As cleavage orientation with respect to the bedding changes, the minimum principal axis for both AMS and APV rotates accordingly.

continental sandstone and silt of Maastrichtian to Lutetian age supporting flexural sequences of Bartonian age (Ellenberger, 1967; Plaziat, 1984). This cover, together with the Paleozoic substratum, is involved in large ramp-related folds (Averbuch et al., 1992; Frizon de Lamotte et al., 1997; Grelaud et al., 2000; Souque et al., 2003). At the regional scale the folds exhibit an 'en-échelon' pattern relative to the North Pyrenean Front, locally called 'nappe des Corbières orientales'.

The 'Chaudrons fold' is an E–W-trending anticline, 3 km wide and 9 km long, involving rocks ranging in age from Upper Cretaceous to Upper Paleocene. Three distinct formations are exposed in the area of interest. The oldest exposed rocks are lacustrine limestones of the Rognacian formation (Maastrichtian), conformably covered by clastics (conglomerates and silicoclastic continental deposits) of the Vitrollian formation (Lower Paleocene). As shown by Plaziat (1984), the Vitrollian formation is made up of an accumulation of paleo-soils that hardened before burial so that it was probably almost isotropic at the end of sedimentary compaction. Finally, Upper Paleocene (Thanetian) is represented again by lacustrine limestone. Folding occurred during Upper Eocene (Ellenberger, 1967). Geometrically, the Chaudrons fold is characterized by a steep forelimb between flat foreland and crest (Fig. 2a). The transition between the foreland and the forelimb is exposed in the field but its study is complicated due to collapse structures. On the contrary, the transition between the forelimb and the crest can be continuously followed within the Vitrollian formation, which is the one that was sampled in this study. The back of the fold is offset by normal faults formed during a Late Oligocene–Miocene event and consequently cannot be reached (see Fig. 1).

3. Field and laboratory measurements

Meso-scale (0.1–1 m) data were collected on two outcrops unveiling, respectively, the front limb and the crest of the fold.

Table 1
Magnetic susceptibility and P-wave velocity (dry and water saturated) data in the three sectors of the Chaudrons fold

		Max.	Int.	Min.	σ	$A\%$
1. Crest	AMS ($\times 10^{-06}$)	5.75	5.65	5.17	0.076	10.6
$\phi = 1.5\%$	APV dry (km s^{-1})	5.26	5.18	4.97	0.045	5.7
	APV saturated	5.82	5.81	5.67	0.026	2.6
2. Hinge	AMS	13.89	13.67	13.03	0.120	6.4
$\phi = 1.9\%$	APV dry	4.61	4.47	4.10	0.089	11.8
	APV saturated	5.46	5.35	5.2	0.047	4.7
3. Forelimb	AMS	32.64	32.16	31.24	0.205	4.4
$\phi = 3.1\%$	APV dry	4.5	4.08	3.5	0.188	25
	APV saturated	5.44	5.22	4.89	0.067	10.7

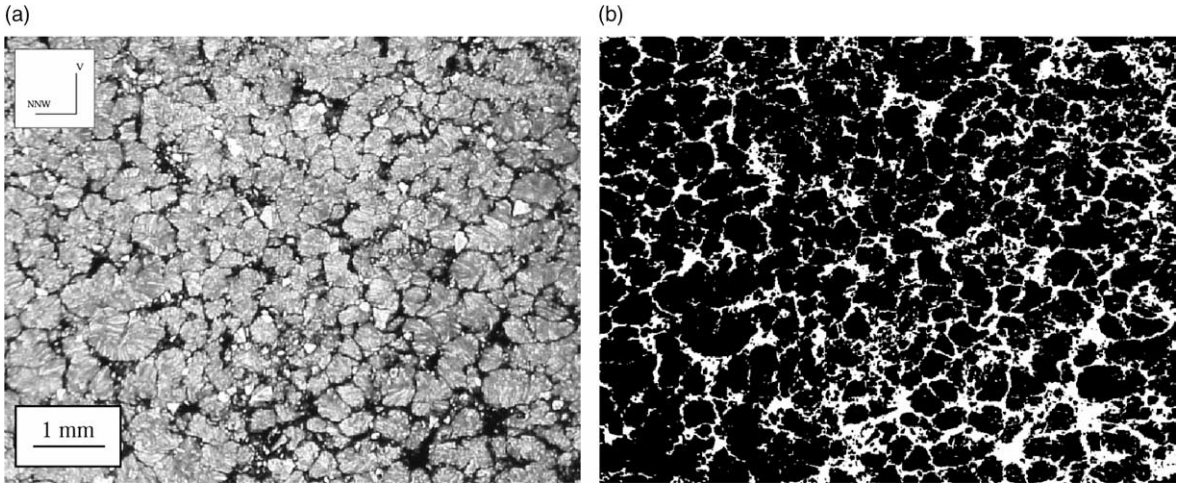

Fig. 4. (a) Microphotograph of a polished section obtained under natural light. The observation plane is vertical and contains the direction of shortening (NNW). On the orientation patch, the letter V stands for 'vertical'. Surface is mostly occupied by grains of microcodium that are embedded in a fine grained clayish matrix. (b) Network formed by the matrix after image threshold. At this scale, no anisotropic pattern emerges.

Both outcrops include a part of the hinge, so that they form together a continuous profile of the Chaudrons fold, backlimb excepted. In the following, we display all results on one unified transect showing the three different panels isolated in Tavani et al. (2004): the crest of the fold, the transition from crest to forelimb (hinge) and the forelimb. The results obtained at sample (cm) scale from AMS and APV measurements are quoted from this former work. The analysis of the microstructures (μm–cm), which provides our new data set, has been performed on polished sections of chips cut from blocks sampled at various locations along the transect. These chips were observed at different magnifications using optical microscopy (reflected light mode) and SEM. In order to infer the composition of the rock in selected zones, X-ray analyses were also conducted.

3.1. Outcrop and sample-scale measurements

The results obtained from outcrop data and AMS/APV estimations were presented in Tavani et al. (2004) and will only be briefly summarized here (Fig. 3 and Table 1). It should be noted, however, that while APV data obtained in samples saturated with water were used in this former work, both dry and saturated results are displayed in the present study. In Tavani et al. (2004), the deformation associated with the development of the Chaudrons anticline was described at two different scales. At the outcrop scale, a very well defined pervasive solution cleavage was observed continuously on the profile (Fig. 2b and c). Using factors such as cleavage spacing, cleavage height over spacing ratio and shape factor of the microlithons, the fold was divided into three sectors in which the relationship between bedding and cleavage varies. In the crest (zone 1 in Figs. 2b and 3), the bedding is nearly horizontal and the cleavage foliation is perpendicular to it. In the hinge (zone 2 in Figs. 2c and 3), the bedding dip progressively increases up to 60°, while the cleavage foliation rotates by 30° only. In the forelimb (zone 3 in Fig. 3), bedding and cleavage dip remain constant. In each of the three panels, AMS and APV measurements displayed rather planar fabrics with the minimum axes parallel to the cleavage pole for both properties, even in zone 2 where an apparent 'top to crest' shearing was observed (Fig. 3). For P-wave velocity measurements, data obtained in dry and water saturated samples show that the increase in stiffness associated with the filling of

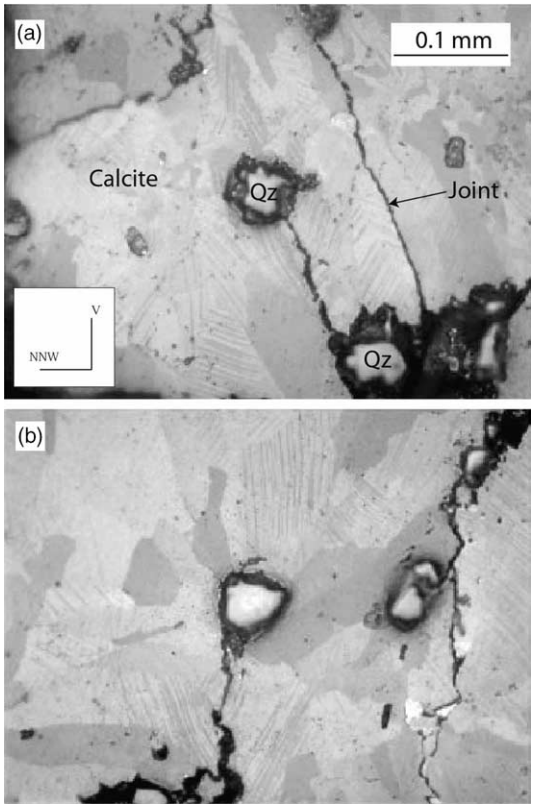

Fig. 5. (a) and (b) Microphotographs of a polished section obtained under reflected light. Three phases, calcite, quartz and ferruginous filling are identified. Quartz grains are inlaid in calcite and the ferruginous matrix that underlines the boundaries between microcodiums also concentrates around quartz inclusions. Inside the microcodiums, many calcite grains are twinned.

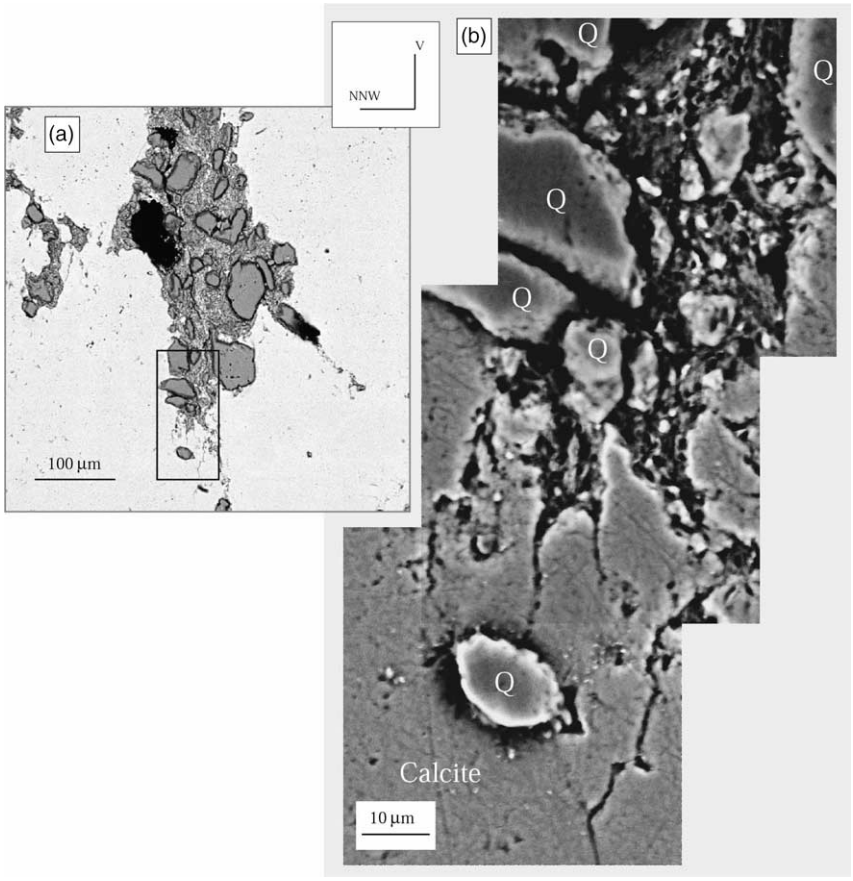

Fig. 6. Scanning electron microscope images (BSE) of a contacting zone between several grains of microcodium. (a) Microcodiums and quartz/clay matrix. (b) Zoom at the transition from calcite to the matrix. An inlaid quartz grain seems to promote the dismantlement of a microcodium.

the pore space does not modify significantly the result in terms of principal directions.

Tavani et al. (2004) suggested that the similarity between AMS and APV was due to solution planes parallel to the macroscopic cleavage that would provide the same kind of anisotropy, despite the fundamentally different origin of the two physical properties. Nevertheless this was not demonstrated in that paper. The authors eventually proposed that the Chaudrons fold had developed in two steps in which macro- and micro-cleavage would have behaved similarly: (1) pre-folding LPS, visible in the crest zone, shaping a set of subvertical solution planes anastomosed at the observation scale, and (2) flexural slip associated with persistent LPS during folding. That interpretation was suggested after the authors had observed an increase in deformation intensity in the forelimb, which was accounted for with persistent layer parallel shortening. Doing so their scenario modified a previous one proposed by Averbuch et al. (1992) in the nearby Lagrasse fold, where cleavage formed during a first step of layer parallel shortening was just passively sheared during folding due to flexural slip.

3.2. Quantitative analysis of the microstructure

The microstructure was analyzed on polished sections cut along a vertical plane parallel to the tectonic transport direction (this plane is the one exhibiting the largest anisotropy for both physical properties and contains the pole to cleavage drawn in Fig. 3). At low magnification (Fig. 4), an observation under natural light of a chip sampled in the forelimb of the fold reveals numerous microcodiums (sets of calcite-rich prisms of organic origin; Bignot, 1994) embedded in an iron- and clay-rich matrix containing dispersed detrital quartz grains. This aggregate, typical in composition of the Vitrollian Formation in the region (Cluzel, 1977; Averbuch et al., 1992), is representative of the intra-microlithon structure, i.e. enclosed between two major cleavage surfaces visible on the outcrops. It is well sorted with low intergranular porosity filled by fine particles. At this scale, no obvious anisotropic pattern that could account for our AMS and APV results is observed. Moreover, statistical investigation such as image autocorrelation (Louis et al., 2005) is made difficult due to a lack of homogeneity (note in Fig. 4 the slight increase in the amount of filling toward the bottom right-hand side of the image).

Under higher magnification, the relationship between microcodiums and quartz grains displays interesting features (Fig. 5). Calcite is clearly the dominating component and quartz grains of less than 50 microns in diameter appear sometimes almost totally embedded. The ferruginous clayish matrix underlines calcite/quartz and calcite/calcite joints. Thickness of the joints seems to vary depending on their type. In calcite, one can still distinguish the aligned prisms

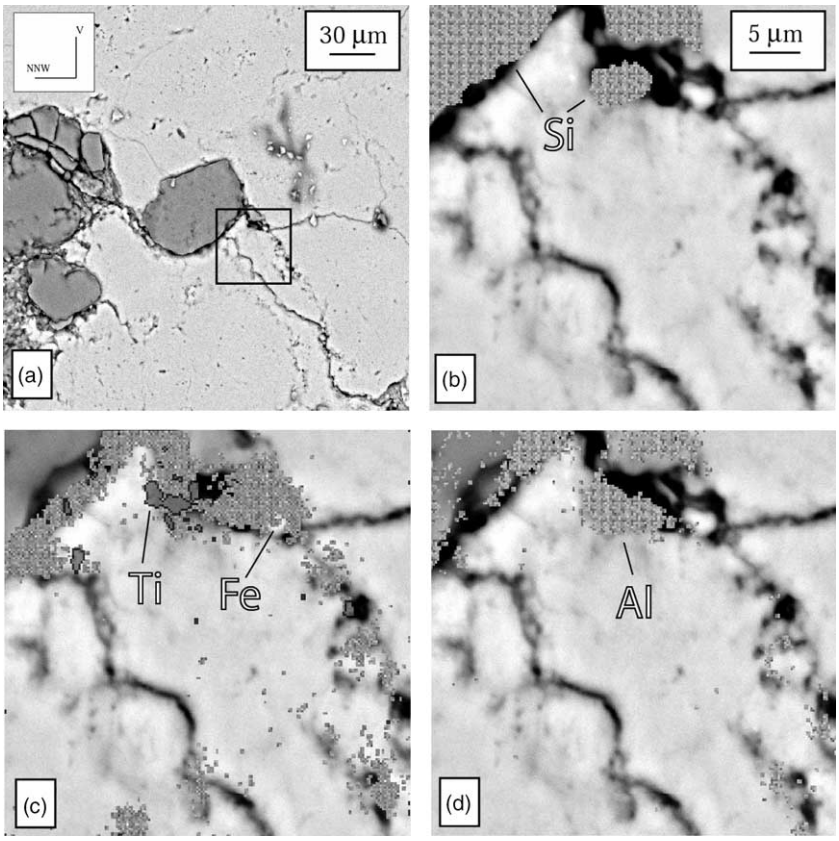

Fig. 7. Scanning electron microscope images and element mapping of a contact zone. (a) General view of the area (BSE). (b) Close view of a contacting zone: distribution of Si. (c) Distribution of Fe (yellow) and Ti (red). (d) Distribution of Al. The lack of match between Fe and Al distributions promotes iron oxides rather than clays or micas as Fe providers.

making up the microcodiums, many of them showing twinning patterns. The calcite/calcite joints seem to follow precisely the contours of these prisms.

SEM images from the same sample are shown in Fig. 6. Fig. 6a is a BSE image of the quartz grains and clay matrix filling the space left by microcodiums, which appear welded by places. Among clay minerals, small grains showing high atomic number (likely iron oxides) can be pointed. Dark areas are assumed to be voids left by quartz grains that chipped off during the polishing. Fig. 6b provides a closer look at the upward transition from a suture zone between two calcite grains, to the 'free' quartz and clay matrix (rectangle in Fig. 6a). Non cohesive clay minerals have left the very top of the imaged surface. Starting from the matrix, at least four channels penetrate into calcite, one of them being apparently promoted by the presence of the quartz inclusion at the bottom of the mosaic image.

In order to gain more insight into the potential source for AMS as into the organization mechanism of such microstructure, we also conducted a semi-quantitative analysis of the quartz/calcite and calcite/calcite grain boundaries using an X-ray detector under the SEM. The spatial distribution of elements Si, Fe, Ti, and Al was mapped in a 40-microns-wide window (Fig. 7). In Fig. 7a, a large view from which the analysis area was chosen is shown. Calcite grain boundaries directly connected to the quartz grain in the center of the image appear much wider as compared with other calcite/calcite joints. Diagonal to the analysis window, the pattern of one of the thicker joints evokes the conical-type stylolites described and simulated in a recent work by Gratier et al. (2005). In Fig. 7b, quartz is identified by the silica-rich zone in the top left corner of the analysis window, the remaining bright zones being occupied by calcite (although Ca was not mapped). Fe, Ti, and Al are essentially located within the grain boundaries (Fig. 7c and d) and only Fe and Al are present in a significant amount. While aluminum reflects the location of the matrix clay minerals, areas containing only iron are suggested to locate iron oxides. X-ray diffractometry spectrum measurements performed by Averbuch et al. (1992) in the Vitrollian Formation identified kaolinite and illite as the clay fraction, and haematite as the iron oxide. Anticipating the effect of such mineralogy on the magnetic susceptibility signal if distributed along calcite grain boundaries, we studied statistically the orientation of calcite/calcite joints showing a connection to quartz grains such as the ones seen in Fig. 5.

Quartz grains are often found within a calcite/calcite joint and it is well-known that the presence of hard particles embedded in a softer material modifies the stress field around the inclusions when the material is subjected to an anisotropic stress state such as the one prevailing in our case. One can refer for example to the observations and models provided by Stromgard (1973), Selkman (1983), and Kenkmann and Dresen

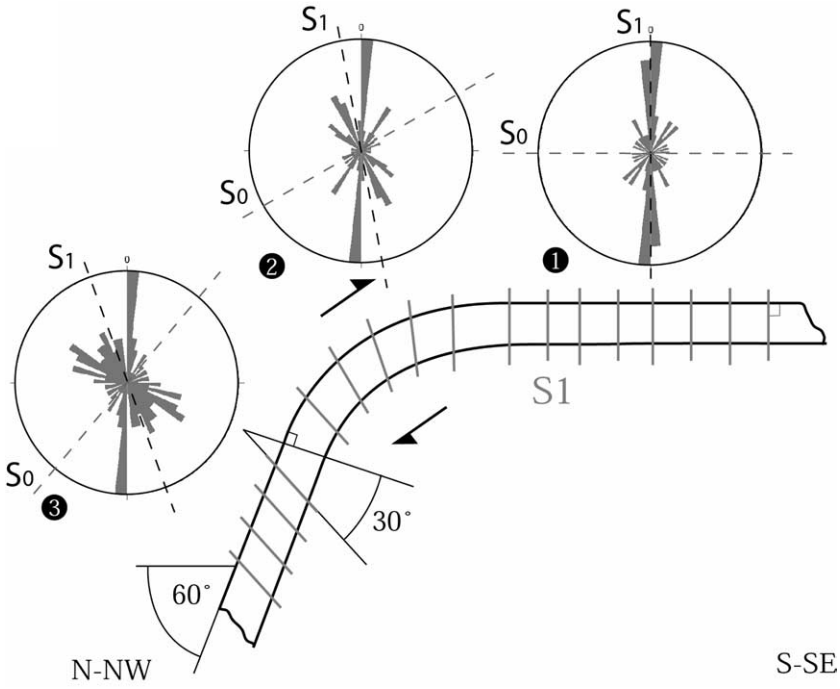

Fig. 8. Same synthetic transect as in Fig. 3, AMS and APV stereoplots are replaced by diagrams showing the dip angle distribution of the 'microcleavage' surfaces. Here the diagrams are parallel to the fold transect. All distributions are highly anisotropic. A vertically oriented set dominates over the fold, and at locations 2 and 3, a second set arises, which is about perpendicular to the bedding plane. At each location, the combination of all the orientations matches fairly well the one of the macrocleavage measured in the field.

(1998). If this is applicable to our study, what implies considering a starting material where quartz grains are already embedded in calcite, an anisotropic pattern is likely to develop with stylolites nucleating at heterogeneities and developing as planar structures perpendicular to the maximum principal stress (Gratier, 1987; Carrio-Schaffhauser et al., 1990).

The orientation distribution of the selected calcite joints in the three sectors of the fold is given in Fig. 8. On each rose diagram, the dipping angles of bedding and macroscopic cleavage planes are recalled. The first striking result is that all the distributions are highly anisotropic, going from the crest to the steep forelimb of the fold. One set of joints, oriented in the vertical direction, dominates over the entire fold. At panels 3 and 2 (forelimb and hinge) another major set appears, roughly perpendicular to the bedding plane (S0), and this set together with the vertical set seems to be bounding a large spectrum of orientations at panel 3 (forelimb). Another interesting feature is that the macroscopic cleavage plane (S1) stands on the bisecting line of all the orientations reported.

4. Discussion

In the following, we show how the microstructural data can explain the APV and AMS fabrics and lead to a better understanding of some of the mechanisms operative during the building of the Chaudrons fold. Based on these new results we finally propose to refine the deformation scenario adopted in Tavani et al. (2004).

4.1. What controls the AMS and APV fabrics, and why are they correlated?

As reported in Fig. 3, a very good match in orientation was observed at all locations between the pole to cleavage and the minimum principal axes of both magnetic susceptibility and P-wave velocity. This observation establishes the presence at the microscopic scale of a feature geometrically similar to the cleavage analyzed by Tavani et al. (2004) at the outcrop scale, controlling both the magnetic and acoustic signals. Anisotropic fabrics always arise from a preferred orientation of lattice, shape or spatial distribution of the rock constituents. Magnetic fabric is usually a function of crystallographic preferred orientation of the minerals and/or grain shape distribution (Hrouda, 1982; Borradaile and Henry, 1997), whereas the anisotropy of P-wave velocity is mainly due, at low effective pressure, to the void space anisotropy (cracks/pores) (Mavko et al., 1998). Regarding the P-wave propagation, in sedimentary rocks, the anisotropy can indeed be strongly influenced by the mean shape of the pore space (Louis et al., 2003): considering the simple case of an elliptic hole embedded in a homogeneous isotropic medium, a maximum compliance will be observed in the direction corresponding to the minor axis of the cavity (Kachanov, 1993). In the context of deformation in its broad sense (i.e. including chemical and mechanical compaction), a planar fabric can have the following origins: preferred orientation of the intergranular contacts and/or preferred orientation of a set of damage patterns like cracks or pressure solution cleavage. A preferred orientation of the

intergranular contacts results, for elastic properties, in a larger stiffness in a direction perpendicular to this preferred orientation (this is the case for the Rothbach sandstone, see Louis et al., 2005). The development of oriented damage features like cracks or solution cleavage under compression can also be easily captured by P-wave velocity measurements. For a set of parallel penny-shaped cracks as well as in the case of cleavage planes, P-wave velocity is greatly reduced along the normal direction while it remains almost unchanged for in-plane propagation. The sensitivity of AMS to void space anisotropy is not straightforward, and basically the only possibility to get it is when oxides or clay minerals crystallize along discontinuities or coat the pore space. For example, this is the case when clay minerals seal the remaining voids along irregular contacts, or when pressure solution operates in limestone, resulting in concentrating ferromagnetic minerals and paramagnetic clays on solution surfaces (Borradaile and Tarling, 1981). The anisotropic shape of the pores will usually have no influence for AMS measurements unless the pore walls are coated with magnetic minerals (Pfleiderer and Kissel, 1994).

Our microstructural study revealed a significant anisotropy in the orientation distribution of calcite/calcite joints filled with clay and iron oxide (Fig. 8). While trying to discriminate between paramagnetic clays (kaolinite, illite) and haematite to find the major contributor to AMS in the Vitrollian formation, Averbuch et al. (1992) showed that both were significantly influencing the signal. Both phyllosilicates and haematite also bear crystallographic anisotropy resulting in normal-type magnetic fabrics as defined by Rochette et al. (1992): crystallographic control on both susceptibility and grain shape results in maximum (minimum) susceptibility along the long (short) dimension of the particles. Thus, estimation of the exact proportion of the magnetic signal, respectively carried by para- and ferro-magnetic minerals (following, for example, the method proposed by Hrouda, 1994), is not critical here since both species are expected to behave similarly during deformation.

Let us consider any single joint. Although all magnetic minerals are obviously not contained in such a location since matrix aggregates are also often observed at the junction of more than two microcodiums (Fig. 4), the preferred joint orientation together with its probable tectonic origin makes it a very suitable feature to give account for both magnetic and acoustic anisotropies. Given its flat shape and knowing that it may have formed perpendicular to the maximum principal stress, the effect of spatial distribution and rotation of the para- and ferro-magnetic grains perpendicular to the flattening direction are expected to produce a planar AMS fabric with a minimum axis perpendicular to the joint. Our microstructural study highlighted more than one set of such joints, and the way signals arising from each single joint sum up to give the observed fabric deserves comment. Analytical and experimental studies of the composition of two elemental fabrics of magnetic susceptibility, which is known to be well described by a second rank tensor (Daly, 1970; Housen et al., 1993; Louis, 2003), established a few important results:

(i) The composition of two elemental fabrics perpendicular to each other conserves the same pair of principal axes as the original fabrics.
(ii) The composition of two identical (same intensity and anisotropy) elemental fabrics at an angle $<90^\circ$ to each other has a maximum intensity axis oriented along the angle bisecting the two original maximum intensity axes.
(iii) When the two elemental fabrics have random orientation and different values of intensity and anisotropy, the orientation of the composition is a simple function of these three parameters.

An acceptable assumption in the case we are studying is to attribute the same intensity and anisotropy to each identified joint. Doing so, the composition of elemental AMS fabrics that builds the stereoplots shown in Fig. 3 can be explained with the same simple argument as that used for the orientation of the macroscopic cleavage, placing the maximum susceptibility axis along the mean of the distribution of all orientations.

For the acoustic properties, the anisotropy of P-wave velocity has to be linked to compliance anisotropy of the rock through its composition and the distribution of its constituents. The joints that we observed can be assimilated to crack-like features filled with a low cohesion material, acting as planes of weakness with respect to the elastic properties. In such a situation, considering that no other source of elastic anisotropy is present, this set of discontinuities is expected to act with respect to P-wave velocities in the same way as a set of cracks parallel to each other. In the P-wave tensor approximation proposed by Louis et al. (2004), this will lead to a planar fabric with a minimum velocity axis perpendicular to the average joint orientation. Following the same argument as for AMS results, we can finally suggest that the preferred orientation of the analyzed joints is a good candidate for the origin of both the P-wave velocity and magnetic susceptibility anisotropies observed in our samples, and that these microstructural observations provide a satisfactory explanation for the excellent correlation between magnetic and elastic fabrics.

As far as AMS is concerned, other potential sources of magnetic susceptibility could have been suggested such as ferroan calcite or ferromagnetic minerals embedded in calcite. In the first case, however, ferroan calcite was recognized to exhibit inverse fabrics with a maximum susceptibility axis tending to cluster around the flattening axis (Rochette et al., 1992), which would not have been consistent with the fabric observed in the Chaudrons fold. Concerning the presence of ferromagnetic grains embedded in calcite, their passive concentration and/or neo-crystallization along the solution surfaces (Evans et al., 2003) is expected to override the signal that could be arising from a preferred orientation inside the crystal.

4.2. What is the formation mechanism of the preferentially oriented joints in calcite?

Pressure solution was clearly operative during the formation of the fold. Evidence can be found in the geometrical

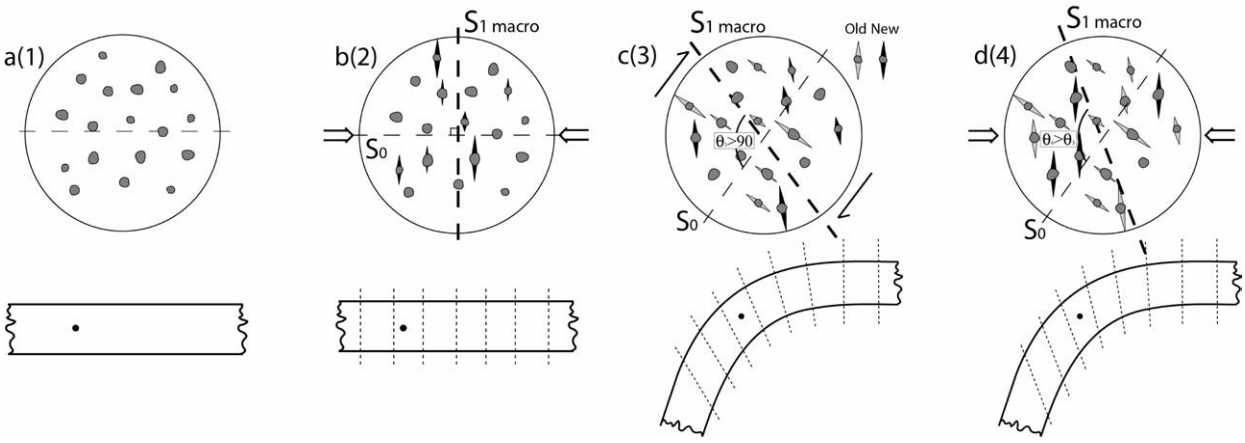

Fig. 9. Micro- and mesoscale scenarios proposed in this study for the accommodation of deformation in the Chaudrons fold: compaction is controlled by horizontal compaction in steps 2 and 4 and by bed parallel shear in step 3. After LPS (step 2), instead of a rotation of the former solution surfaces, new sets are produced, which are perpendicular to the contemporaneous maximum compressive stress.

relationship between adjacent calcite grains (Fig. 5b) that reminds us of stylolites in carbonates (Renard et al., 2004; Gratier et al., 2005), or in the grain joints that resemble the pattern of concentration of insoluble material at grain boundaries (Borradaile and Tarling, 1981; Evans et al., 2003). In the blocks sampled, calcite veins about 1 mm thick were found, and Cluzel (1977) showed in the Vitrollian Formation that calcite would dissolve against quartz grains and recrystallize in pressure shadows perpendicular to the direction of shortening. Finally, pressure solution is the easiest deformation mechanism to operate in calcite, at low temperature and stress levels below the one necessary for twinning to occur (<10 MPa; Engelder and Marshak, 1985). Since twinning was observed in our samples, the stress level required for pressure solution has consequently been attained.

When studying the orientation distribution of calcite/calcite joints, we justified the selection of the ones that were contacting a quartz grain by arguing that the presence of stress heterogeneity may trigger and/or promote the development of solution surfaces (Carrio-Schaffhauser et al., 1990) and therefore reflect the deformation history. Also, Stromgard (1973) and Kenkmann and Dresen (1998) have shown that the stress distribution around a high viscosity particle embedded in a lower viscosity material is modified, and that different stress patterns may be obtained depending on the coupling conditions at the interface. In all cases this interaction results in a lowered mean stress close to the hard inclusion and along a plane perpendicular to the applied stress. If we transpose these ideas to our case, the joints reported in our microstructural study could correspond to a combination of solution surfaces with void space generation in the close vicinity of the quartz inclusions where stress concentration was lower, in response to the application of an anisotropic stress field. While this scheme is plausible, the presence of the inclusion itself inside a matrix of calcite deserves further discussion.

Suppose we have an original homogeneous aggregate of microcodiums, clay and quartz grains with no particular initial organization. One can suggest that compression is going to organize the microstructure so that microcodiums will be pressed against one another, occasionally trapping a quartz grain. The resulting sutures should be mostly located along a plane perpendicular to the direction of compression. When quartz grains are trapped in these sutures, the pattern of quartz grain with adjacent calcite/calcite joint (Fig. 5) would be durable due to the mechanical effect of the rigid inclusion discussed earlier. Therefore the population of joints studied in Fig. 8 may in fact be seen as an inventory of the quartz trapping surfaces during successive compressive events recorded in the Chaudrons fold. In order to reflect the state of the whole microstructure and then explain the AMS and APV results, these surfaces have to be stated as representative of the whole population of intergranular contacts in the rock.

Concerning potential fluid flow associated with the development of the macroscopic cleavage, Tavani et al. (2004) suggested that the Chaudrons fold had been structured as an open system, based on the scarcity of veins and on the porosity data given in Table 1, showing an increase in average porosity towards the forelimb. Although quantitative geochemical analyzes for assessing potential water advection ($\delta^{18}O$), metasomatism, or Ca depletion for volumetric strain estimation would provide more definite answers (Davidson et al., 1998), a high solution rate can be assumed from the microstructure analyzed in this study. Engelder and Marshak (1985) reported that a proportion of quartz–clay matrix of 10% or more can provide an efficient network for diffusion of dissolved material up to the free fluid system of the rock. A direct estimate from Fig. 4b gives a cement proportion of about 20–25%, which suggests that this case may have applied in the Chaudrons fold.

4.3. What scenario may account for the microcleavage pattern in the Chaudrons fold?

In the work presented by Tavani et al. (2004), the pattern displayed by the macroscopic cleavage was accounted for with a combination of LPS and flexural slip, LPS being responsible for generating a set of surfaces perpendicular to the bedding, which was eventually sheared in the forelimb due to increasing

flexural slip. As the ratio of bed height over cleavage spacing, as well as the shape factor of the microlithons, increases towards the forelimb, the authors suggested that LPS even persisted in this sector during fold growth. The microstructural observations reported in the present study can help in refining this scenario. The orientation analysis in Fig. 8 revealed two major sets of joints, one being perpendicular to the bedding and the other one vertical along the fold. This single observation suggests that the cleavage pattern at the scale of the microstructure is more complex than first imagined, in that it is not consistent with the concept of a single set of joints generated before fold activation and then passively rotated during bed parallel shear. Taking advantage of the microstructural study conducted in this paper, Fig. 9 puts forth a scenario in four steps for the sequential formation of preferentially oriented sets of solution cleavage surfaces in the Chaudrons fold. The observation plane is perpendicular to the fold axis. In the intact rock (Fig. 9a), quartz grains are distributed homogeneously in the calcite-bearing rock and no initial anisotropy is assumed. In step 2 (Fig. 9b), LPS driven by horizontal compressive stress forms a first set of quartz bearing joints, the amount of which would be directly proportional to the local volume loss. At this stage, the orientation of the macroscopic cleavage is perpendicular to the bedding. Fold starts growing during step 3 (Fig. 9c) with flexural slip (Tavani et al., 2004), as expected in the forelimb of fault bend and fault propagation anticlines (Suppe, 1983; Suppe and Medwedeff, 1990). The bedding is progressively tilted while entering the forelimb and at the scale of the microstructure bed parallel shear generates a new set of quartz related solution surfaces oriented accordingly at an angle $>90°$ to the bedding. The direct consequence on the orientation of the macroscopic cleavage is a rotation toward a new angle to bedding $\theta_3 > 90°$ bisecting the angle between the new microcleavage and the one inherited from LPS. The vertical set of quartz bearing joints might have formed after fold growth ended since its presence is insensitive to the location inside the structure. Its appearance corresponds to step 4 of our scenario and is shown in Fig. 9d. The mechanism is the same as for LPS except that the bedding is tilted. In the forelimb, the effect on the macroscopic cleavage is an apparent further rotation with respect to the bedding towards an angle $\theta_4 > \theta_3$.

As a result, the microstructures associated with the formation of the fold itself appear much less developed than pre- and post-folding features, which can be expected since shortening on a fault or detachment surface is favored as the fold grows. Still, due to the nature of internal strain accommodation, a full record of the various deformation events experienced by the Vitrollian formation inside the Chaudrons fold was observed. And the evolution towards the forelimb of the angle of the macroscopic cleavage with respect to the bedding is now better understood.

5. Conclusion

In this work we completed a multiscale study of the deformation patterns exhibited by the Chaudrons fold, providing new elements arising from observations of the microstructure. First, these observations allowed us to account for the fabric displayed by AMS and APV measurements, as well as for the geometrical match between them. We identified grain joints statistically oriented parallel to the outcrop-scale cleavage in which the presence of poorly cohesive material and magnetic phases generated planar fabrics for both AMS and APV. Second, we investigated the potential mechanism presiding over the formation of such a microstructural pattern. We suggested that two processes might have operated in unison: (1) pressure solution and twinning occurred in calcite due to horizontal compaction of the rock mass; (2) the presence of quartz grains enhanced dissolution of calcite and induced stress heterogeneities favoring the preservation of joints along a plane preferentially oriented perpendicular to the contemporary maximum principal stress. Finally, a refined scenario depicting the progressive development of the cleavage inside the Chaudrons fold was proposed. We consider that the microstructural processes are the same before, during and after folding, ruling out passive shearing of a set of solution surfaces formed during LPS. And we support the hypothesis that pressure solution and preservation of non welded interfaces in shadow zones located in the vicinity of quartz inclusions is operative throughout the deformation history of the fold, giving rise to a range of diversely oriented discontinuities which were not reworked once formed.

Acknowledgements

This work has been supported by a research agreement between Institut Français du Pétrole and University of Cergy-Pontoise. The authors thank F. Salvini and S. Tavani from Roma III University and C. Souque from University of Cergy-Pontoise for helpful discussions and participation in the early stage of the work. SEM imagery was handled by Omar Boudouma (UMR CNRS 7072, Universite Paris VI) and we thank him for these high quality images. This manuscript was greatly improved thanks to insightful reviews by A.M. Boullier, G. Viola and B. Housen.

References

Anastasio, D.J., Fisher, D.M., Messina, T.A., Holl, J.E., 1997. Kinematics of decollement folding in the Lost River Range, Idaho. Journal of Structural Geology 19 (3–4), 355–368.

Averbuch, O., Frizon de Lamotte, D., Kissel, C., 1992. Magnetic fabric as a structural indicator of the deformation path within a fold-thrust structure: a test case from the Corbières (NE Pyrenees, France). Journal of Structural Geology 14 (4), 461–474.

Bignot, G., 1994. L'énigme des Microcodium. Bulletin de la Société géologique de Normandie, 25–45.

Borradaile, G.J., Henry, B., 1997. Tectonic applications of magnetic susceptibility and its anisotropy. Earth Science Reviews 42, 49–93.

Borradaile, G.J., Tarling, D.H., 1981. The influence of deformation mechanisms on magnetic fabrics in weakly deformed rocks. Tectonophysics 77 (1–2), 151–168.

Carrio-Schaffhauser, E., Raynaud, S., Latière, H.J., Mazerolle, F., 1990. Propagation and localization of stylolites in limestones. In: Knipe, R.J.,

Rutter, E.H. (Eds.), Deformation Mechanisms, Rheology and Tectonics Journal of the Geological Society of London Special Publications 54, pp. 193–199.

Cluzel, D., 1977. Etude microtectonique de l'avant-pays de la nappe des Corbières orientales (Aude-France). Unpublished PhD thesis, Université Paris-Sud.

Daly, L., 1970. Etude des propriétés magnétiques des roches métamorphiques ou simplement tectonisées. Nature de leur aimantation naturelle. Détermination de leur anisotropie magnétique et application à l'analyse structurale. PhD thesis, Université Pierre et Marie Curie (Paris VI).

Davidson, S.G., Anastasio, D.J., Bebout, G.E., Holl, J.E., Hedlund, C.A., 1998. Volume loss and metasomatism during cleavage formation in carbonate rocks. Journal of Structural Geology 20 (6), 707–726.

Ellenberger, F., 1967. Les interférences de l'érosion et de la tectonique tangentielle tertiaire dans le Bas-Languedoc: note sur les charriages cisaillants. Revue de Géologie Dynamique et de Géographie Physique 9, 87–142.

Engelder, T., Marshak, S., 1985. Disjunctive cleavage formed at shallow depths in sedimentary rocks. Journal of Structural Geology 7 (3–4), 327–343.

Evans, M.A., Lewchuk, M.T., Elmore, R.D., 2003. Strain partitioning of deformation mechanisms in limestones: examining the relationship of strain and anisotropy of magnetic susceptibility (AMS). Journal of Structural Geology 25 (9), 1525–1549.

Frizon de Lamotte, D., Mercier, E., Dupré la Tour, A., Robion, P., Averbuch, O., 1997. Cinématique du plissement et déformation interne des roches. L'exemple du pli de Lagrasse (Aude, France). Comptes-rendus de l'Académie des Sciences 324 (IIa), 591–598.

Frizon de Lamotte, D., Souque, C., Grelaud, S., Robion, P., 2002. Early record of tectonic magnetic fabric during inversion of a sedimentary basin. Short review and examples from the Corbières transfer zone (France). Bulletin de la Société Géologique de France 173 (5), 461–469.

Gratier, J.-P., 1987. Pressure solution deposition creep and associated chemical differentiation in sedimentary rocks. In: Jones, M.E., Preston, R.M.F. (Eds.), Deformation Mechanisms in Sediments and Sedimentary Rocks Journal of the Geological Society of London Special Publications 29, pp. 25–38.

Gratier, J.-P., Muquet, L., Hassani, R., Renard, F., 2005. Experimental microstylolites in quartz and modeled application to natural stylolitic structures. Journal of Structural Geology 27, 89–100.

Grelaud, S., Buil, D., Hardy, S., Frizon de Lamotte, D., 2000. Trishear kinematic model of fault-propagation folding and sequential development of minor structures: the Oupia anticline (NE Pyrenees, France) case study. Bulletin de la Société Géologique de France 171 (4), 441–449.

Housen, B.A., Richter, C., van der Pluijm, B.A., 1993. Composite magnetic anisotropy fabrics: experiments, numerical models and implications for the quantification of rock fabrics. Tectonophysics 220, 1–12.

Hrouda, F., 1982. Magnetic anisotropy of rocks and its application in geology and geophysics. Geophysical Surveys 5, 37–82.

Hrouda, F., 1994. A technique for the measurement of thermal changes of magnetic susceptibility of weakly magnetic rocks by the CS-2 apparatus and KLY-2 Kappabridge. Geophysical Journal International 118, 604–612.

Kachanov, M., 1993. Elastic Solids with Many Cracks and Related Problems Advances in Applied Mechanics, vol. 30. Academic Press, Boston, MA, pp. 259–445.

Kenkmann, T., Dresen, G., 1998. Stress gradients around porphyroclasts: palaeopiezometric estimates and numerical modelling. Journal of Structural Geology 20 (2–3), 163–173.

Louis, L., 2003. Anisotropies microstructurales composites dans les roches réservoir: Conséquences sur les propriétés élastiques et relation à la déformation. PhD thesis, Université de Cergy-Pontoise, France.

Louis, L., David, C., Robion, P., 2003. Comparison of the anisotropic behaviour of undeformed sandstones under dry and saturated conditions. Tectonophysics 370 (1–4), 193–212.

Louis, L., Robion, P., David, C., 2004. A single method for the inversion of anisotropic data sets with application to structural studies. Journal of Structural Geology 26, 2065–2072.

Louis, L., David, C., Metz, V., Robion, P., Menendez, B., Kissel, C., 2005. Microstructural control on the anisotropy of elastic and transport properties in undeformed sandstones. International Journal of Rock Mechanics and Mining Science 42 (7–8), 911–923.

Mavko, G., Mukerji, T., Dvorkin, J., 1998. The Rock Physics Handbook—Tools for Seismic Analysis in Porous Media. Cambridge University Press, Cambridge.

Pfleiderer, S., Kissel, C., 1994. Variation of pore fabric across a fold–thrust structure. Geophysical Research Letters 21 (19), 2147–2150.

Plaziat, J.C., 1984. Le domaine pyréneen de la fin du Crétacé à la fin de l'Eocène. Stratigraphie, paléo-environnements et évolution paléo-géographique. Thèse de doctorat, Université Paris Sud Orsay (Paris XI).

Renard, F., Schmittbuhl, J., Gratier, J.-P., Meakin, P., Merino, E., 2004. Three-dimensional roughness of stylolites in limestones. Journal of Geophysical Research 109, B03209. doi:10.1029/2003JB002555.

Rochette, P., Jackson, M.J., Aubourg, C., 1992. Rock magnetism and the interpretation of anisotropy of magnetic susceptibility. Reviews of Geophysics 30, 209–226.

Saint-Bézar, B., Hebert, R.L., Aubourg, C., Robion, P., Swennen, R., Frizon de Lamotte, D., 2002. Magnetic fabric and petrographic investigation of hematite-bearing sandstones within ramp-related folds: examples from the South-Atlas Front (Morocco). Journal of Structural Geology 24, 1507–1520.

Selkman, S., 1983. Stress and displacement distributions around pyrite grains. Journal of Structural Geology 5 (1), 47–52.

Souque, C., Robion, P., Frizon de Lamotte, D., 2002. Cryptic magnetic fabric of tectonic origin revealed by heating of sedimentary samples from the Corbières, France. Physics and Chemistry of the Earth (A) 27, 1253–1262.

Souque, C., Frizon de Lamotte, D., Leturmy, P., Robion, P., 2003. Duplex at the lateral tip of a thrust fault: the "La Cagalière" example (NE Pyrenees, France). Geodinamica Acta 16 (2–6), 89–98.

Stromgard, K.E., 1973. Stress distribution during formation of boudinage and pressure shadows. Tectonophysics 16, 215–248.

Suppe, J., 1983. Geometry and kinematics of fault-bend folding. American Journal of Science 283, 684–721.

Suppe, J., Medwedeff, D.A., 1990. Geometry and kinematics of fault-propagation folding. Eclogae Geologicae Helvetiae 83, 409–454.

Tavani, S., Louis, L., Souque, C., Robion, P., Salvini, F., Frizon de Lamotte, D., 2004. Folding related fracture pattern and physical properties of rocks in the Chaudrons ramp-related anticline (Corbières, France). In: Swennen, R., Roure, F., Granath, J. (Eds.), Deformation, Fluid Flow and Reservoir Appraisal in Foreland Fold and Thrust Belts. AAPG Hedberg series no. 1.

Tavarnelli, E., 1997. Structural evolution of a foreland fold-and-thrust belt: the Umbria–Marche Apennines, Italy. Journal of Structural Geology 19 (3–4), 523–534.

Thorbjornsen, K., Dunne, W.M., 1997. Origin of a thrust-related fold: geometric vs. kinematic tests. Journal of Structural Geology 19 (3–4), 303–319.